NATIONAL ADVISORY COMMITTEE FOR AERONAUTICS

TECHNICAL NOTE 3098

DENSITY PROFILES OF SUBSONIC BOUNDARY LAYERS ON A FLAT PLATE DETERMINED BY X-RAY AND PRESSURE MEASUREMENTS

By Ruth N. Weltmann and Perry W. Kuhns

Lewis Flight Propulsion Laboratory
Cleveland, Ohio

Washington
February 1954

NATIONAL ADVISORY COMMITTEE FOR AERONAUTICS

TECHNICAL NOTE 3098

DENSITY PROFILES OF SUBSONIC BOUNDARY LAYERS ON A FLAT PLATE DETERMINED BY X-RAY AND PRESSURE MEASUREMENTS

By Ruth N. Weltmann and Perry W. Kuhns

SUMMARY

Laminar, transitional, and turbulent boundary layers were investigated in a subsonic wind tunnel at Mach numbers of 0.55 and 0.78 at various Reynolds numbers and stations along a flat plate. Comparisons are made of the density profiles obtained with a total-pressure probe of small frontal opening and by means of an X-ray absorption method and, in a few cases, by using interferometer data. The limitations of the probe and X-ray methods are discussed.

The decrease in mass flow in the tunnel due to the insertion of the pressure probe was found to affect the pressure measurements in the boundary layer. A mass-flow correction for the pressure data is suggested. The maximum difference between the mass-flow corrected pressure profiles and the radiation measurements was 0.8 percent in density ratio. No change in boundary-layer type from transitional to turbulent or from laminar to transitional was observed when the probe was inserted into the boundary layer.

INTRODUCTION

Density profiles are most frequently obtained by total-pressure-probe measurements. They can also be measured by using radiation methods, such as X-ray absorption (refs. 1 and 2) and light interference (ref. 3). A comparison of density boundary layers obtained by those three methods seems especially interesting since there are several differences between the probe method and any radiation method: (a) In probing, a foreign body of finite size is introduced into the air stream, whereas nothing involved in a radiation method interferes with the flow; (b) the probe measures local pressures, integrating over the width of its frontal opening, whereas a radiation method provides an integration over the entire tunnel span and is valid only to the extent that the flow is two-dimensional; (c) the radiation methods measure density ratios directly, whereas the probe total pressures are converted into densities

on the general assumptions of constant static pressure and constant total temperature through the boundary layer along a line normal to the airfoil surface. Thus, the extent of agreement between the results of probe and of radiation methods is determined by at least four considerations: the amount of disturbance created in the boundary layer by the insertion of a probe, the validity of assuming two-dimensional flow in the tunnel, and the validity of assuming constant static pressure and constant total temperature through the boundary layer on a flat plate at any given station.

In this paper, experimental density profiles obtained from total-pressure-probe and X-ray absorption measurements are presented and compared with profiles obtained from interferometer data taken by D. R. Buchele and W. L. Howes at the NACA Lewis laboratory. For the radiation methods, the probe was retracted. The boundary layers were measured on a flat-plate airfoil in a subsonic wind tunnel of two-dimensional flow. Laminar, transitional, and turbulent boundary layers are presented as obtained at Mach numbers of 0.55 and 0.78 with Reynolds numbers from 0.2×10^6 to 2.9×10^6. The limitations of the two methods are discussed.

APPARATUS AND TECHNIQUE

Wind Tunnel and Airfoils

The boundary-layer measurements were made in a subsonic wind tunnel on two flat-plate airfoils. The rectangular test section had a span of 3.8 inches and a height of 10.0 inches. The flat plates were mounted at midheight, were about 17 inches long, and extended over the complete tunnel span. Plate I was 1/4 inch thick and had a curved leading edge on its lower surface only, while plate II was 1/2 inch thick and had a symmetrically curved leading edge (fig. 1). The air intake and exhaust facilities limited this tunnel to a maximum Mach number of 0.78. The inlet-air temperature was controlled by heaters and was adjusted to remain close to room temperature (about 540° R) under all operating conditions. The air flow could be adjusted to give static operating pressures from about 1/10 to 1 atmosphere. Static-pressure taps were provided along the upper and lower tunnel walls and along the upper surfaces of the flat plates at regular intervals to determine pressure gradients. Thermocouples were mounted along the upper plate surfaces to obtain temperature measurements.

Total-Pressure Probe

Provisions were made in the top wall of the tunnel for insertion of a total-pressure probe, at various longitudinal stations, to traverse the boundary layer by means of a micrometer feed. The contact of the

probe with the flat plate was indicated by closure of an electric circuit between the probe and the plate. The total-pressure probe (fig. 1) was designed for least disturbance of the flow in the tunnel and the boundary layer. For this reason, the probe support was 1.25 inches downstream of the probe opening, and the probe opening was made as small as possible, but large enough for the probe to respond rapidly to pressure changes. Thus, the scanning height of the frontal opening was chosen to be 0.002 inch and the probe casing, to be 0.001 inch thick. The opening width was approximately 0.014 inch. The pressure measured on contact was assumed to be the pressure at the center line of the probe-opening height. The pressure was read on a manometer filled with acetylene tetrabromide of calibrated density which indicated the difference between the total pressure in the boundary layer and the free-stream total pressure.

X-Ray Radiation Equipment

The arrangement of the X-ray source and receiver, in relation to the wind-tunnel test section, is shown schematically in figure 2 and photographically in figure 3. The X-ray absorption technique has been described previously in references 1, 2, and 4 to 6, so that only the most important features of the setup and method are discussed here.

The X-ray source was a Machlett type A-2 diffraction tube with a tungsten target and beryllium windows. It was powered by a commercial full-wave rectified and filtered power supply at a voltage between 3 and 4 kilovolts, which gave a continuous spectrum at an average wavelength of 3 to 4 angstroms. The X-rays were bounded by a 0.010- by 0.25-inch slit next to the beryllium window and passed through a 0.001-inch-thick cellophane window into the test section. At the receiving side of the tunnel, there was a 0.005- by 0.25-inch slit covered by a 0.001-inch-thick cellophane window. The receiver was a Geiger-Mueller tube having a mica end window and was connected to commercial counting equipment. In most cases, it was necessary to use argon-filled tubes to obtain sufficient counting efficiency at the low X-ray voltages used. Both the X-ray source and receiver and their slits and windows were mounted on movable steel plates (fig. 3) which were part of the tunnel sides. These plates were slid past adjacent side plates of the tunnel in order to scan the boundary layer. The positioning was accurate to within 0.001 inch. The X-ray intensity of the beam after passing through the wind tunnel outside the boundary layer compared with the intensities observed when the boundary layer was scanned gave a direct indication of the relative density changes in the boundary layer.

In order to ascertain the position of the slits through which the X-ray beam passes relative to the surface of the flat plate, the slits were moved past the flat plate and above it while X-ray intensity

measurements were made. The solid line in figure 4 shows a schematic curve which should be obtained from such an experiment. However, before this experiment can be started, the slits have to be alined in relation to each other. The alinement is made by moving only one slit past the flat plate while the other slit remains stationary somewhere above the plate. A curve similar to the solid line shown in figure 4 should result, where the distance from zero to full intensity equals the slit width. All these experiments are made without air flowing over the plate. For the curves given in figure 4, the slits had been previously alined relative to each other, and the distance y is the distance of the slit center line above the surface of the plate. With the slits alined, full intensity was obtained at $y = 0.003$ inch. It is felt that the distance y is inaccurate within ± 0.0005 inch as a result of misalinement and other mechanical inaccuracies.

When the flat plate had a polished surface, the dashed curve of figure 4 was obtained. This result indicated that some of the X-rays were specularly reflected by the plate toward the exit slit and thus were picked up by the receiver, so that the measured intensity was the sum of the transmitted beam intensity and the reflected beam intensity. Since X-rays reflect only at grazing angles, the additional component due to the reflected intensity decreases with increasing slit distance y from the plate. The position of the maximum intensity of the reflection is a function of the X-ray wave length, since the angle of reflection varies with wave length. All attempts to eliminate reflections were unsuccessful, but the reflections could be made ineffective by diffusing them. The diffusion was accomplished by a very slight roughening of the surface of the flat plate by means of a slight vapor blast. Then, a curve similar to the solid line in figure 4 was obtained having the expected shape to within the statistical error. Although the surface roughness of the plate was sufficient to diffuse the reflected X-rays, it apparently did not interfere with the flow, since the density profiles, as obtained with the total-pressure probe before and after vapor blasting, check within 0.2 percent in density ratio.

In addition to alining the slits, it is necessary to obtain the product of mass absorption coefficient B and tunnel span L for each given set of tunnel and X-ray conditions. From the classical absorption law,

$$\ln(I_1/I_2) = BL(\rho_2 - \rho_1) \tag{1}$$

(For convenience, all symbols are defined in appendix A.) Thus, after each boundary layer was scanned, BL was obtained for the given set of X-ray conditions by measuring the X-ray intensity at various static tunnel pressures with the slit far outside the boundary layer. The value of BL was then obtained from a plot of equation (1) on semilogarithmic paper as the slope of the resulting straight line.

CALCULATIONS OF PROFILES AND ERRORS

Total-Pressure Probe

The conventional assumption was made that the static pressure is constant through the boundary layer in a direction normal to the plate surface. The Mach number and density distributions could then be calculated from the ratio of total to static pressure by means of the isentropic-flow equation.

$$\frac{\rho}{\rho_0} = \frac{t_0}{t} = \frac{T_0}{T} \frac{\left(1 + \frac{\gamma - 1}{2} M^2\right)}{\left(1 + \frac{\gamma - 1}{2} M_0^2\right)} = \frac{T_0}{T} \left(\frac{P}{P_0}\right)^{\frac{\gamma-1}{\gamma}} \tag{2}$$

For subsonic flow, the additional assumption might be made that the total temperature in the boundary layer is constant along a line normal to the plate surface. Since then $T_0/T = 1$, the density profile can be expressed directly in terms of the Mach number distribution or of the measured total-pressure ratios.

The total-pressure probe was calibrated at known pressures in a jet to determine the pressure deviation due to an error in angular positioning. At angular vertical displacements of less than 10° and at angular horizontal displacements of less than 5°, the error was less than 1.0 percent. Since the total-pressure probe was rotated before each measurement to yield a minimum differential reading against the total pressure in the plenum chamber, the angular error must have been so small as to make the pressure error due to an angular displacement negligible. The pressure differential could be read within ±0.01 inch of mercury. Two or three pressure probings were made on each boundary layer which yielded an experimental precision of about 0.2 percent in density ratio ρ/ρ_0. The uncertainty in the position of the probe relative to the flat plate may account for a total error of 0.001 inch in distance y from the plate. It is felt that these experimental errors in probing could be decreased, but no effort was made in this direction since the experimental errors of the X-ray method are even greater, as will be shown, and since in comparing two methods the accuracy of comparison is determined by the larger error of the less accurate method.

Another experimental error, which is also extremely small, is due to the fact that the probe has a finite width of 0.002 inch; consequently, the measured pressure is integrated over this width, so that in a pressure gradient the measured pressure is not fully equal to the pressure at the center of the probe frontal area (ref. 7). In addition

to the experimental errors in probing, errors might be introduced in the assumptions for equation (2) of constant total temperature and constant static pressure over the boundary-layer profile at a given station.

X-Ray Measurements

The difference between the density along one beam path passing through the tunnel in the free stream well outside the boundary layer and the density along another beam path traversing the tunnel within the boundary layer can be obtained from intensity measurements of both beams at the receiver side by using the logarithmic intensity-density relation for absorption of radiation through media of given density and thickness. The equation for the density profile can then be given as

$$\rho/\rho_0 = 1 - \ln(I/I_0)/BL\rho_0 \tag{3}$$

The coefficient B, being a function only of X-ray tube voltage for a given setup, is obtained for each density profile by the previously described calibration method (eq. (1)). For $\Delta I/I << 1$, equation (3) can be approximated by

$$\rho/\rho_0 = 1 - (\Delta I/I_0)/BL\rho_0 \tag{4}$$

where $\Delta I = I - I_0$.

The error in density ratio, which can be obtained from equation (4), depends on the accuracy with which the intensities are measured. Since intensities are composed of single events which occur in a statistical pattern, the higher the measured intensity the greater will be the accuracy of its measurement. Because of instrumental restrictions (refs. 1 and 8), very high intensities can be obtained only by counting for a long period of time. On the other hand, long-period electronic and aerodynamic drifts might change tunnel and X-ray conditions. A compromise was found by scanning repeatedly up and down through the boundary layer so that each point is composed of ten 1-minute counting periods. In this manner, three to four boundary layers were studied for each given tunnel condition. The final density profiles (figs. 5 to 7) are obtained from an average of all those measurements. The density ratio ρ/ρ_0 thus determined ranged in probable error from ± 0.3 to ± 0.9 percent. The errors differed somewhat, depending on the intensity, density, and voltage (refs. 1 and 8).

Another error is introduced by the fact that the scanning slits are of finite width. Consequently, the measured intensity is the intensity integrated over this width. From calculations shown in appendix B and figure 8, this error is always less than ±0.2 percent for the test conditions used to obtain the density profiles shown in figures 5 to 7.

Another additional error when boundary layers are measured by means of any radiation method is introduced by the presence of boundary layers on both tunnel sides. From calculations given also in appendix B, this error is less than -0.2 percent. Since the experimental errors were about ±0.6 percent, the errors due to the slit width and geometry as well as the error introduced by the presence of boundary layers on the tunnel walls were considered small and thus were neglected.

RESULTS AND DISCUSSION

Static-Pressure Distribution on Flat Plates

The static-pressure distribution along flat plates I and II, with both types of leading edge, was measured. The static-pressure gradient along plate I was found to be almost constant at each inlet condition. A typical pressure profile is shown in figure 9. Because of the limitations of the test conditions, it was impractical to investigate laminar boundary layers on plate I, because transition was too close to the leading edge. Hence, other means had to be found to obtain transitional and laminar boundary layers. Reference 8 suggests that the transition Reynolds number on a flat plate can be increased by providing an increasing static-pressure gradient along the plate. This can be accomplished by providing a curved leading edge on the surface of the airfoil. In accordance with this suggestion, flat plate II was utilized, with the result that the static-pressure gradient changed greatly along the upstream end of the plate, as can be seen in figure 9. A survey of boundary layers along this plate showed that all boundary layers at stations beyond $x = 6.74$ inches, corresponding to Reynolds numbers of 0.5×10^6 to 2.9×10^6, were of the turbulent type. At station $x = 2.74$ inches, the boundary layers with Reynolds numbers between 0.5×10^6 and 1.1×10^6 were of a transitional type (fig. 6), whereas the boundary layers at station $x = 1.24$ inches with Reynolds numbers between 0.2×10^6 and 0.5×10^6 were of a laminar type (fig. 7).

Mass-Flow Blockage Due to Probe Insertion

Typical static-pressure distributions along flat plate II and along the tunnel walls are shown in figures 9 and 10, respectively, for the flow conditions obtained before and after a total-pressure probe was inserted in the tunnel to probe a boundary layer with the values of air

inlet and exhaust pressures fixed. The change in static pressure was the result of a mass-flow blockage caused by the probe support and is a function of the ratio between the tunnel cross-sectional area and the frontal probe-support area. Reference 10 gives values for relative static-pressure changes and for Mach number changes due to probe-support blockage which agree rather well with the data obtained in this work. Figures 9 and 10 were obtained with the total-pressure probe at a distance x of 2.74 inches from the leading edge of flat plate II and with a tunnel static pressure close to atmospheric. The shaft of the probe, whose dimensions are shown in figure 1, was located about 1.25 inches behind the station, somewhat ahead of the point where the static pressure along the upper tunnel wall is a minimum.

The blockage resulted in an increased static pressure throughout the tunnel cross section at the point of probe insertion, as can be seen in figures 9 and 10 or, effectively, in a decreased free-stream Mach number. Since the static pressure is assumed to be constant throughout the boundary layer, the effective free-stream Mach number of the tunnel can be found from the ratio between the static pressure at the wall and the total pressure in the upstream plenum chamber. This is, then, the free-stream Mach number M_0 for which the boundary-layer density profile has been determined by using equation (2). Without the probe, however, the mass flow is greater, and a lower static pressure results, accompanied by a higher free-stream Mach number M_0. Thus, with no changes assumed in air-inlet and outlet pressures, the boundary-layer density profile measured without the probe has been obtained at a higher Mach number than the profile measured with the probe. In order to compare both density profiles at the same free-stream Mach numbers, one of the profiles has to be corrected to the free-stream Mach number M_0 of the other profile.

Since it was found that the mass-flow change caused by insertion of the probe did not measurably affect the Reynolds number, the boundary-layer thickness could be assumed to remain constant. The corrections can then be made by using the following relation which is derived from equation (2):

$$(\rho/\rho_0)_{M_2} = K' + K''(\rho/\rho_0)_{M_1} \tag{5}$$

where

$$K' = \frac{(\rho_w/\rho_0)_{M_2} - (\rho_w/\rho_0)_{M_1}}{1 - (\rho_w/\rho_0)_{M_1}}$$

and

$$K'' = \frac{1 - (\rho_w/\rho_0)_{M_2}}{1 - (\rho_w/\rho_0)_{M_1}}$$

Comparison of Density Profiles

The X-ray and total-pressure-probe density profiles, calculated by means of equations (2) and (3), are plotted in figures 5 to 7. All the density profiles determined from the total-pressure-probe measurements have been corrected by using equation (5) to the same free-stream Mach number M_0 as existed when the radiation measurements were made. The magnitude of this correction is shown in figure 11, where the mean density values of the corrected and uncorrected pressure-probe data and the mean X-ray values are plotted for the density profile of figure 6 at a Reynolds number of 1.1×10^6.

The profiles from figure 6 are compared with those obtained from interferometer measurements when the identical tunnel and flat plate II are used under essentially the same flow conditions. The interferometer data were corrected for refraction errors (ref. 3) and for tunnel sidewall boundary layers and corner effects. Since the total-pressure-probe data (calculated from eq. (2)) assume constant total temperature across the boundary layer, the mean values of the shaded density profiles (fig. 6) have been corrected, as indicated by the dashed lines, for a total-temperature variation across the boundary layer in accordance with reference 11. However, the uncertainty of this correction is difficult to evaluate. The interferometer profile and the total-temperature corrected probe data are also replotted in figure 11 for the flow condition presented there in order to facilitate comparison.

Figure 5 gives the density distribution of turbulent boundary layers for Mach numbers of 0.78 and 0.55 at Reynolds numbers from 0.5×10^6 to 2.9×10^6 and at two distances x of 3.375 and 7.375 inches from the leading edge of flat plate I. The density is plotted in a dimensionless manner as a density ratio ρ/ρ_0. The distance from the flat plate y is also plotted nondimensionally as a distance ratio y/x.

The same system of plotting was used for the transitional boundary layers in figure 6, which were obtained for Mach numbers of 0.78 and 0.55, Reynolds numbers of 1.1×10^6 and 0.5×10^6, and at a distance x of 2.74 inches from the leading edge of flat plate II. Laminar profiles are shown in figure 7 for Mach numbers of 0.78 and 0.55, Reynolds numbers of 0.5×10^6 and 0.2×10^6, and at a distance x of 1.24 inches from the leading edge of flat plate II. The hatched area indicates the region of probable experimental error in the pressure-probe data, while the length and width of the rectangles indicate the probable experimental

errors of the X-ray measurements, and the dotted area on figure 6 indicates the probable experimental error in the interferometer data.

The differences between density boundary layers obtained with the total-pressure probe and corrected for mass-flow blockage and those determined by the X-ray method for essentially the same flow condition are apparently within the errors of the experiment. Although the differences between the probe profiles and the interferometer data are of about the same magnitude as the ones between the X-ray and probe data, they are somewhat larger than can be explained by the experimental errors of these two methods. On the other hand, the largest observed difference in density ratio ρ/ρ_0 between the pressure and radiation methods is only about 0.8 percent; this value is usually considered to be a good check when several independent methods are used for the same measurement, especially since, for technical reasons, the measurements could not be taken simultaneously. As a result, the flow conditions might not have been entirely identical, although all precautions were taken to obtain the same flow and test conditions. Thus, the observed differences can be due to all or some of the following reasons: (1) experimental errors, (2) differences in flow and test conditions, (3) flow disturbance created in the boundary layer by the insertion of the probe, (4) uncertainty in the mass-flow correction of the probe data, (5) invalidity of the assumption of two-dimensional flow, (6) invalidity of the assumption of constant static pressure and constant total temperature across the boundary layer, and (7) uncertainty in the total-temperature correction of the probe data as applied in figure 6. These considerations make it difficult to conclude how much of the difference in density ratio (≤ 0.8 percent) is due to the flow disturbance created by the insertion of the probe and how much is due to the other six possible reasons. However, the experiments indicate definitely that the disturbance created by the probe was not enough to effect a change from transitional to turbulent or from laminar- to transitional-type boundary layers.

As an experimental method, the total-pressure-probe method has definite advantages over the X-ray radiation method. The instrumentation is simple and straightforward, and no special skill is required in making the measurements. A complete boundary-layer profile can be evaluated, with the necessary calculations included, in a few minutes; whereas the X-ray method requires expensive instrumentation, mechanical precision, and several hours to make one boundary-layer determination, with even less accuracy than that obtained almost automatically when a probe is used. In addition, the assumption of two-dimensional flow is not required for use of the total-pressure probe, whereas this assumption is a requisite for all radiation methods.

Lewis Flight Propulsion Laboratory
National Advisory Committee for Aeronautics
Cleveland, Ohio, November 9, 1953

APPENDIX A

SYMBOLS

The following symbols are used in this report:

A	constant
a	width of exit slit
B	mass absorption coefficient
b	width of entrance slit
C	distance from entrance slit to entrance side of tunnel
I	X-ray intensity
L	tunnel span
M	Mach number
P	total pressure
p	static pressure
s	distance along beam path through medium
T	total temperature
t	static temperature
x	distance from leading edge of plate along airfoil
y	distance of slit center line above surface of plate
z	variable distance along tunnel span
δ_s	boundary-layer width at tunnel side
γ	ratio of specific heats, 1.4
ρ	density

Subscripts:

M_1, M_2	referring to free-stream conditions with and without mass-flow blockage by probe support, respectively
w	referring to wall and plate surface conditions
0	referring to free-stream conditions
1,2	referring to other than free-stream conditions

APPENDIX B

ERRORS IN X-RAY MEASUREMENT

Finite Slit Sizes

The classical equation for the intensity I' of one beam through a medium of variable density is

$$I' = A' \exp\left[-B\int_0^s \rho(y)ds\right] \tag{B1}$$

The total intensity I is obtained by integrating the intensity I' of the individual beams from one point in the entrance slit over the width of the exit slit and then integrating this over the width of the entrance slit

$$I = A\int_{y_0-\frac{b}{2}}^{y_0+\frac{b}{2}} dy_2 \int_{y_0-\frac{a}{2}}^{y_0+\frac{a}{2}} dy_1 \exp\left[\frac{-B(C+L)}{y_1 - y_2}\int_{y_1-\frac{L}{C+L}(y_1-y_2)}^{y_1} \rho(y)dy\right] \tag{B2}$$

where y is the variable distance normal from the flat plate; y_0 is the distance of the center line of the slits from the plate; y_1 is the variable distance on the exit side; and y_2 is the variable distance on the entrance side.

By expanding $\rho(y)$ in terms of $\rho(y)$ at $y = y_0$ to the second derivative of the density with respect to y and integrating the expanded equation, the following approximate equation is obtained for the error in the density measurement ρ at any distance y due to the finite slit sizes:

$$\frac{\Delta\rho}{\rho} = K\frac{1}{\rho}\left(\frac{d^2\rho}{dy^2}\right)_{y=y_0} \tag{B3}$$

where

$$K = \frac{a^2}{24}\left[1 - \frac{L}{C+L} + \frac{1}{3}\frac{L^2}{(C+L)^2} + \frac{b^2L^2}{72(C+L)^2}\right]$$

For figure 8 the errors in density due to the finite slit width are calculated as a function of y for the conditions of the experimental setup ($a = 5\times10^{-3}$ in., $b = 10^{-2}$ in., and $C = L = 3.8$ in.) and for values of $\rho_w/\rho_0 = 0.85$ and 0.95, which are representative for the subsonic flow region of $0.5 \leq M \leq 0.8$. For the computations resulting in figure 8, $\rho(y)$ was calculated from equation (2) by using the 1/7-power velocity-distribution equation (ref. 12) to represent turbulent and transitional flow, and $\rho(y)$ was calculated from equation (2) by using the Blasius velocity-profile equation (ref. 13) to represent laminar flow. The two error lines on figure 8 represent extremes, so that all errors of the experimentally measured density profiles are less than those indicated by the two curves.

Boundary Layers on Tunnel Sides

If z is the spanwise vector and $\rho(z)$ is the boundary-layer profile on the tunnel sides with a boundary-layer width of δ_s, then the intensity of a beam passing through the tunnel at any point is given by

$$I = A \exp\left[-B\rho(y)L\right] \exp\left[2B\int_0^{\delta_s} \rho(y)-\rho(z)\right] dz$$

$$\simeq Ae^{-B\rho(y)L}\left[1 + \epsilon B\rho(y)L\right] \tag{B4}$$

where

$$\epsilon = \frac{2}{L}\int_0^{\delta_s}\left[1 - \frac{\rho(z)}{\rho(y)}\right]dz \tag{B5}$$

and

$$\frac{\Delta\rho(y)}{\rho_0} \simeq \frac{-1}{B\rho_0 L}\left(\frac{\Delta I}{I_0}\right) + \epsilon_0 - \epsilon \tag{B6}$$

Since the usual form for $\Delta\rho(y)/\rho_0$ as derived from equation (4) is

$$\frac{\Delta\rho(y)}{\rho_0} \simeq -\frac{1}{B\rho_0 L}\left(\frac{\Delta I}{I_0}\right)$$

the error due to both tunnel-side boundary layers is

$$\frac{\Delta\rho}{\rho} \simeq \epsilon_0 - \epsilon \tag{B7}$$

Equation (B5) is solved by assuming a turbulent boundary layer on both tunnel sides such as

$$\rho(z) = \rho_w + \left[\rho(y) - \rho_w\right]\left(\frac{z}{\delta_s}\right)^{2/N} \tag{B8}$$

and designating $\delta_{s,0}$ as the tunnel-side boundary-layer thickness in the free stream outside the interference from the boundary layer of the plate. The equation for the error in density ratio is then

$$\left|\frac{\Delta\rho}{\rho}\right| \leq \left|\frac{4}{N+2}\left[\frac{\delta_{s,0}}{L}\left(1 - \frac{\rho_w}{\rho_0}\right)\right]\right| \tag{B9}$$

By inserting extreme experimental conditions ($\rho_w/\rho_0 = 0.89$ for $M = 0.78$, $N \simeq 10$, and $\delta_{s,0}/L \simeq 5\times10^{-2}$), then

$$\left|\frac{\Delta\rho}{\rho}\right| \leq 0.002 \tag{B10}$$

that is, the error introduced in the density ratio in the experimental boundary layers was always less than -0.2 percent.

3123

REFERENCES

1. Weltmann, Ruth N., Fairweather, Steven, and Papke, Daryl: Application of X-Ray Absorption to Measurement of Small Air-Density Gradients. NACA TN 2406, 1951.

2. Dimeff, J., Hallett, Ralph K., Jr., and Hansen, C. Frederick: X-Ray Instrumentation for Density Measurements in a Supersonic Flow Field. NACA TN 2845, 1952.

3. Howes, Walton L., and Buchele, Donald R.: A Theory and Method for Applying Interferometry to the Measurement of Certain Two-Dimensional Gaseous Density Fields. NACA TN 2693, 1952.

4. Arnold: Dichtemessungen mit Röntgenstrahlen an Überschallströmungen im Windkanal. Archiv. Nr. 66/124, Aerodynamisches Inst., Peenemünde Heeresversuchsstelle, Nov. 1, 1944.

5. Winkler, E. M.: Density Measurements in Supersonic Flow by Means of X-Ray Absorption Method. Jour. Appl. Phys., vol. 22, no. 2, Feb. 1951, pp. 201-202.

6. Arnold: Density Tests on the Structure of Compression Shocks on Wedge-Profiles. Trans. of WVA Rep. Archive No. 192, by Lockheed Aircraft Corp.

7. Gettleman, Clarence C., and Krause, Lloyd N.: Considerations Entering into the Selection of Probes for Pressure Measurement in Jet Engines. Proc. Inst. Soc. Am., vol. 7, 1952, pp. 134-137.

8. Weltmann, Ruth N., and Kuhns, Perry W.: An Analysis of an X-Ray Absorption Method for Measurement of High Gas Temperatures. NACA TN 2580, 1951.

9. Dryden, Hugh L.: Air Flow in the Boundary Layer Near a Plate. NACA Rep. 562, 1936.

10. Krause, Lloyd N., and Gettleman, Clarence C.: Effect of Interaction Among Probes, Supports, Duct Walls and Jet Boundaries on Pressure Measurements in Ducts and Jets. Proc. Inst. Soc. Am., vol. 7, 1952, pp. 138-141.

11. Tucker, Maurice, and Maslen, Stephen H.: Turbulent Boundary-Layer Temperature Recovery Factors in Two-Dimensional Supersonic Flow. NACA TN 2296, 1951.

12. Schlichting, H.: Lecture Series "Boundary Layer Theory." Part II - Turbulent Flows. NACA TM 1218, 1949.

13. Schlichting, H.: Lecture Series "Boundary Layer Theory." Part I - Laminar Flows. NACA TM 1217, 1949.

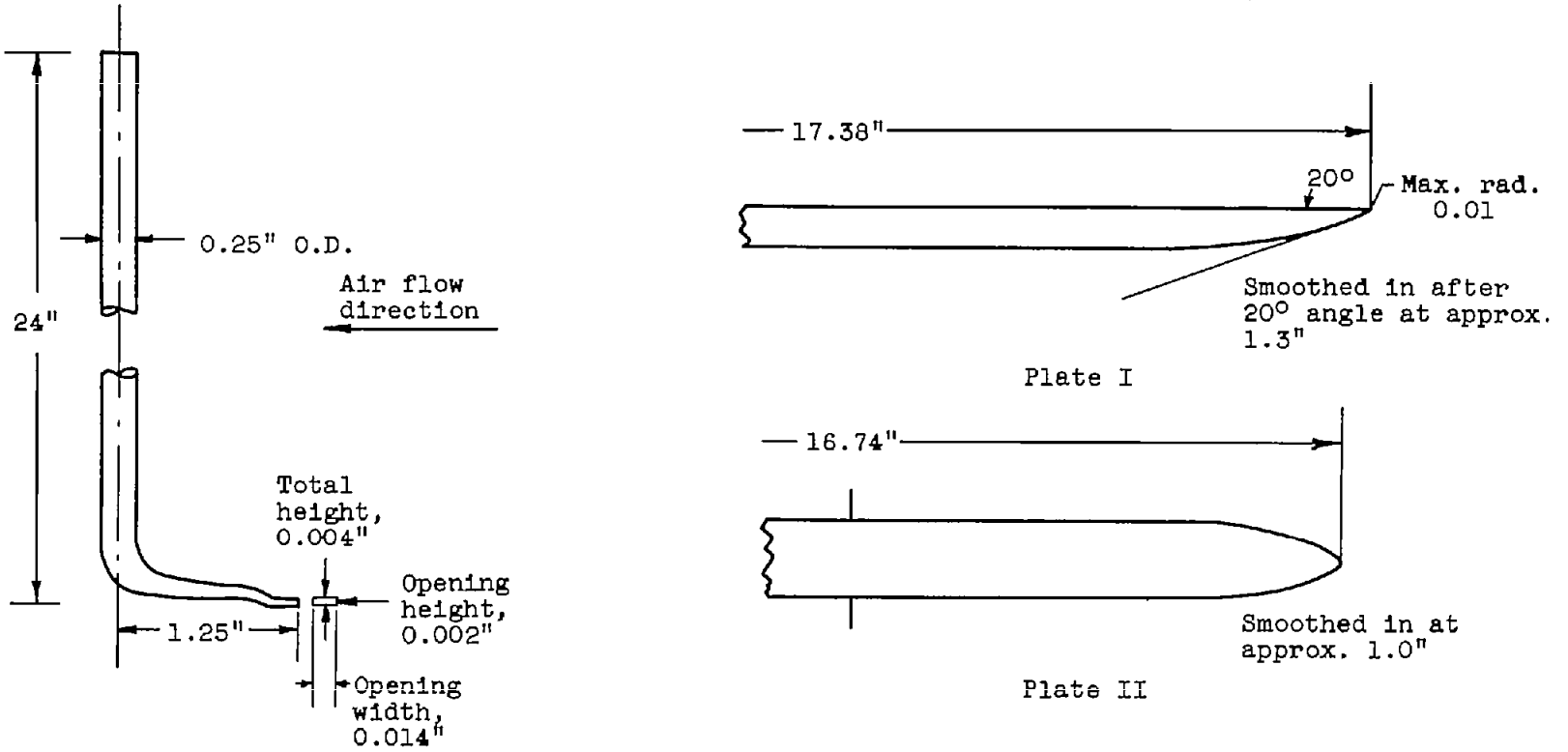

Figure 1. - Flat plates and total-pressure probe.

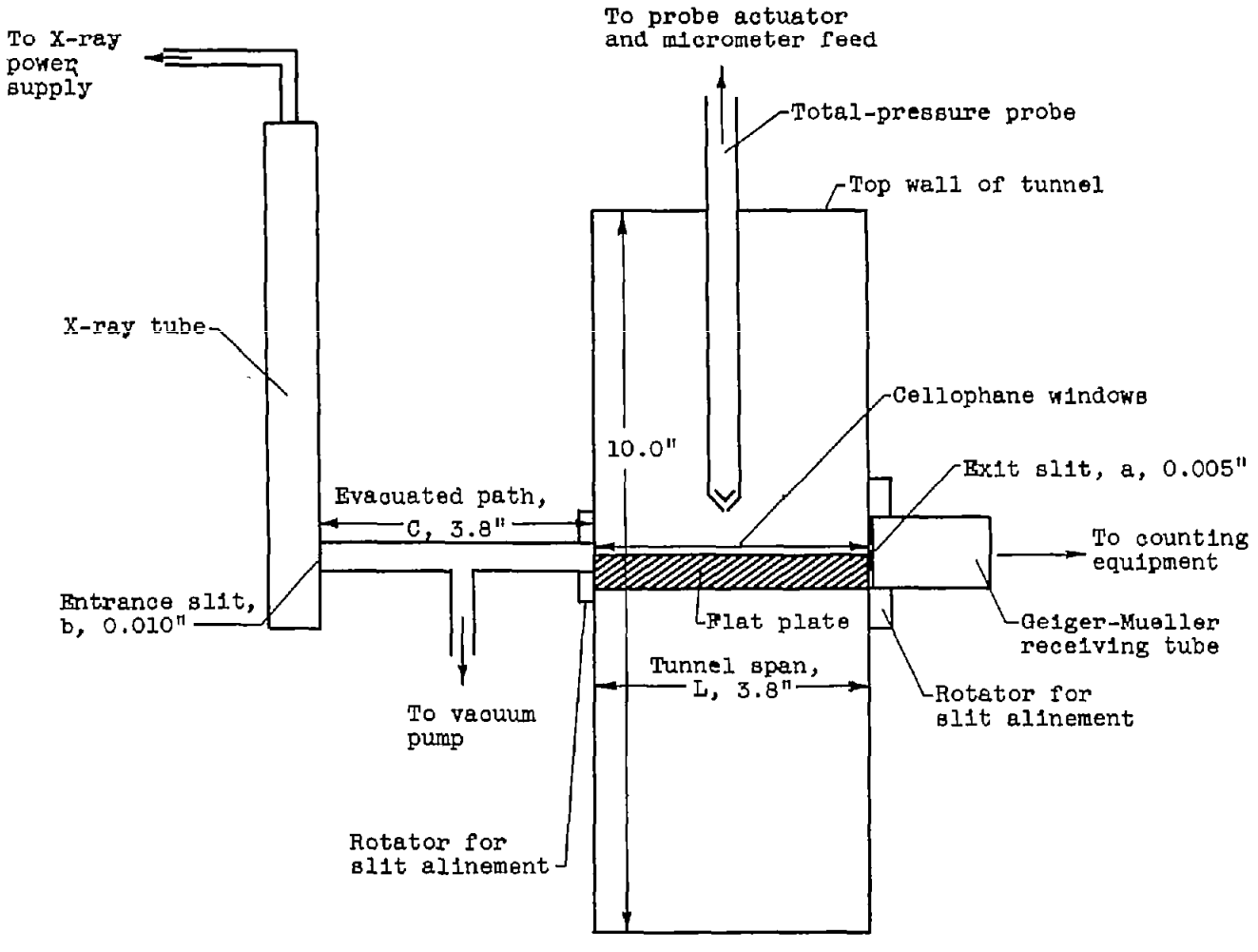

Figure 2. - Schematic arrangement of X-ray radiation equipment.

CX-3 back 3123

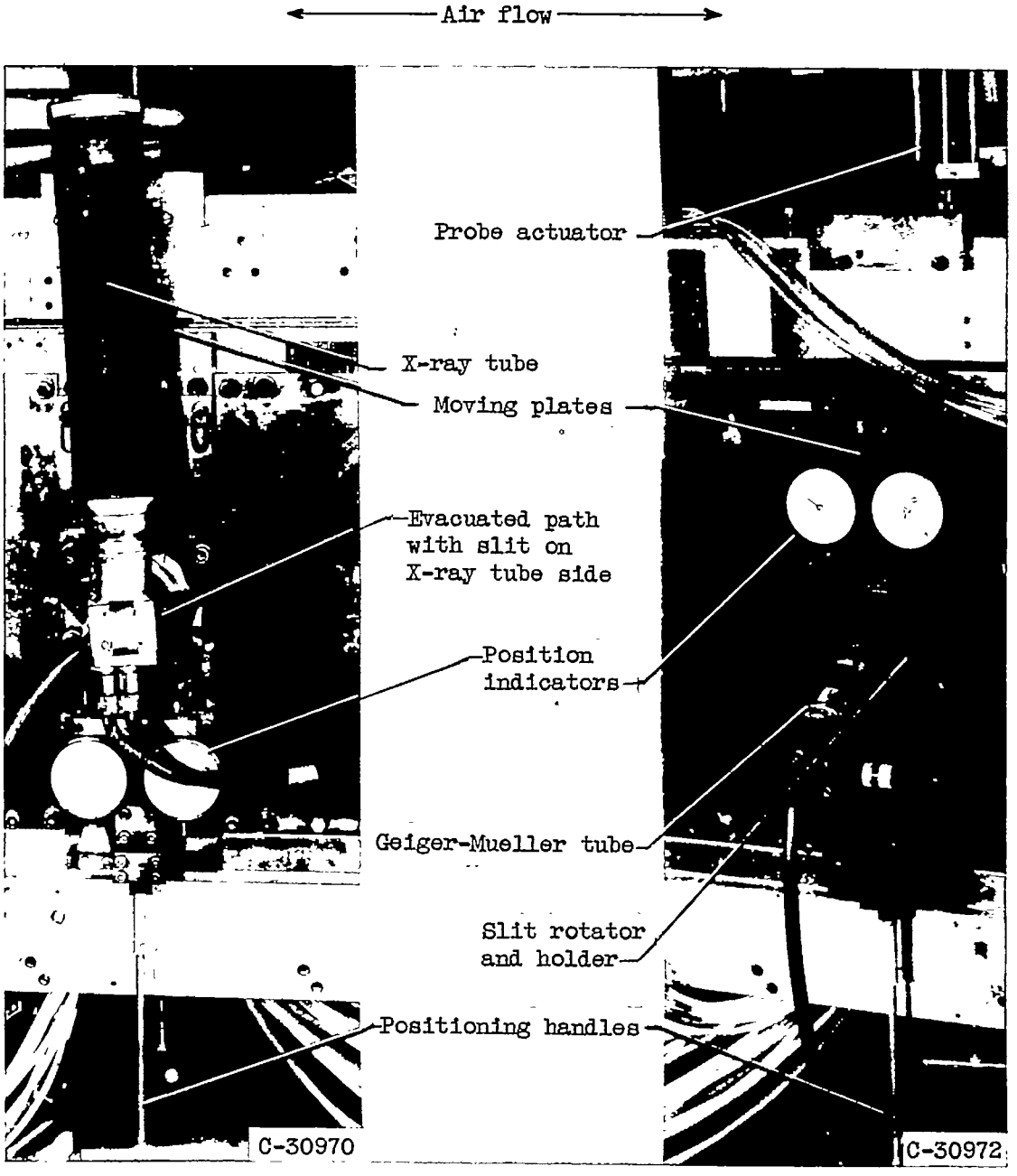

X-ray entrance side with X-ray tube attached to movable plate. Motion measured on indicator scales.

X-ray exit side with Geiger-Mueller receiving tube attached to movable plate. Motion measured on indicator scales.

Figure 3. - X-ray radiation equipment.

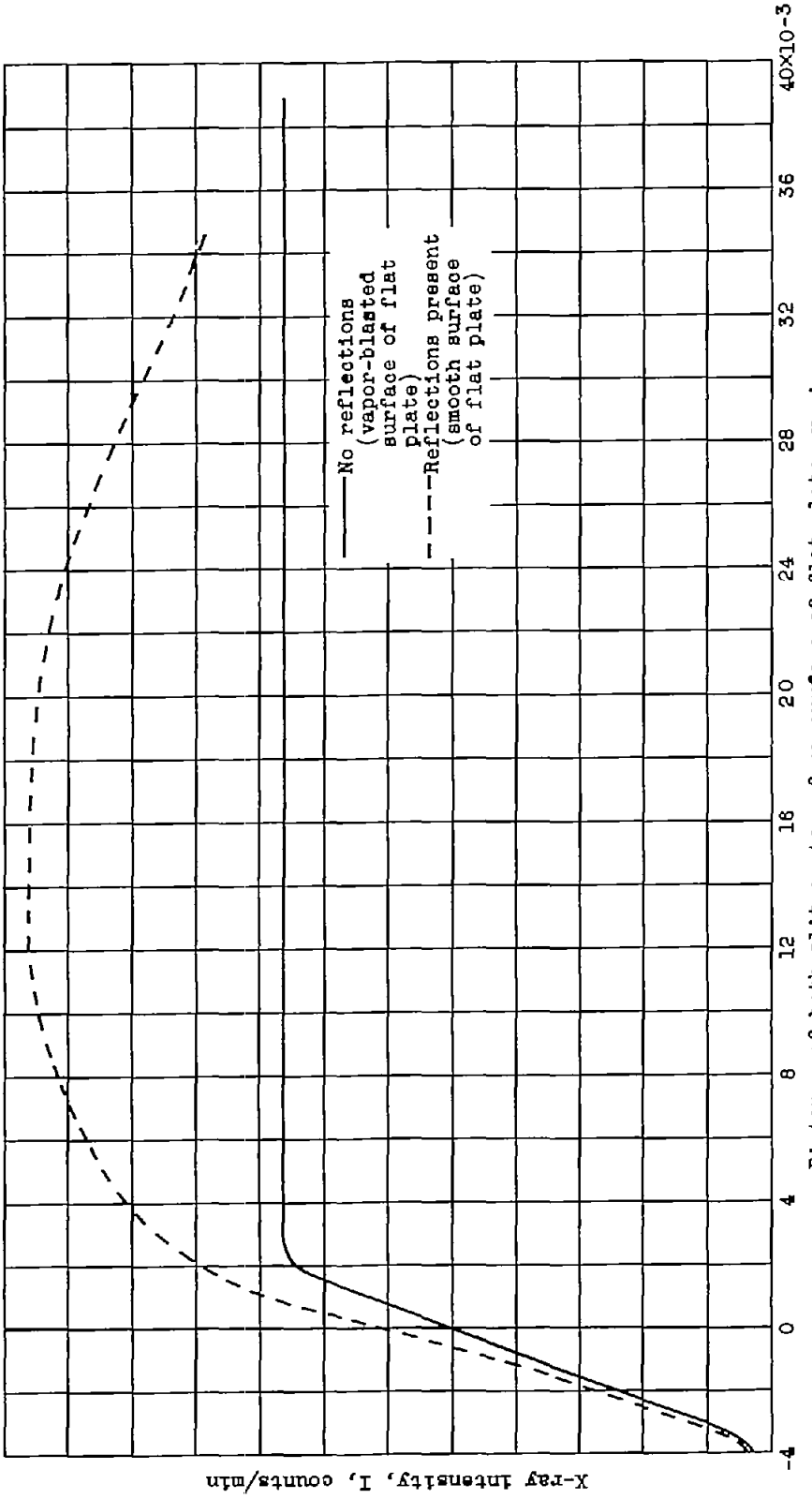

Figure 4. - Schematic calibration curves for slit positioning.

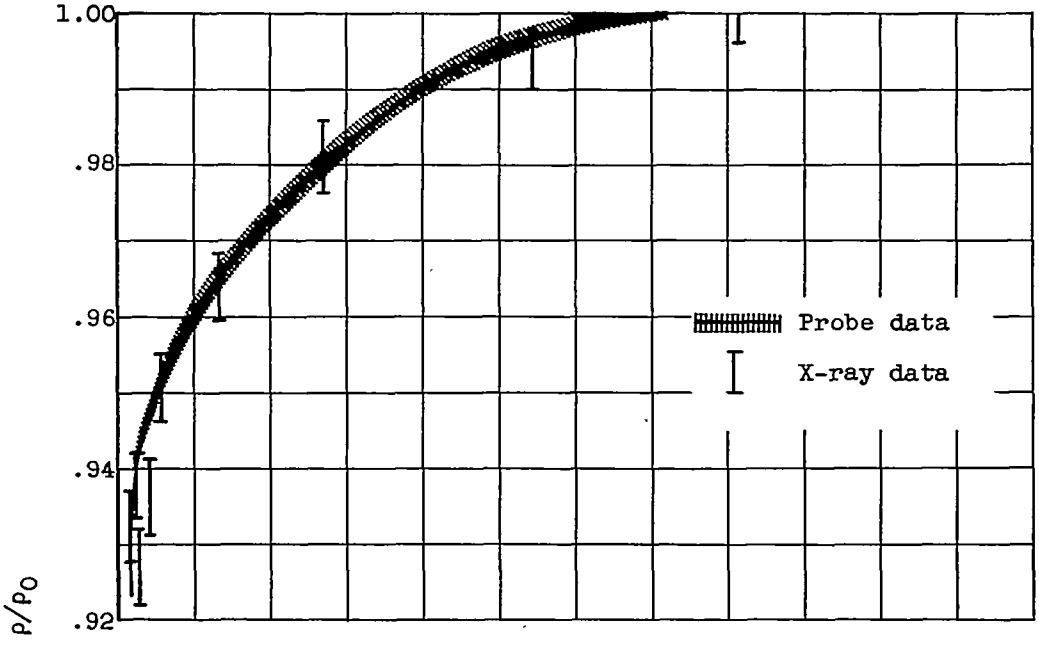

(a) Mach number, 0.78; Reynolds number, 2.9×10^6; static pressure, 24.4 inches of mercury; distance from leading edge of plate, 7.375 inches.

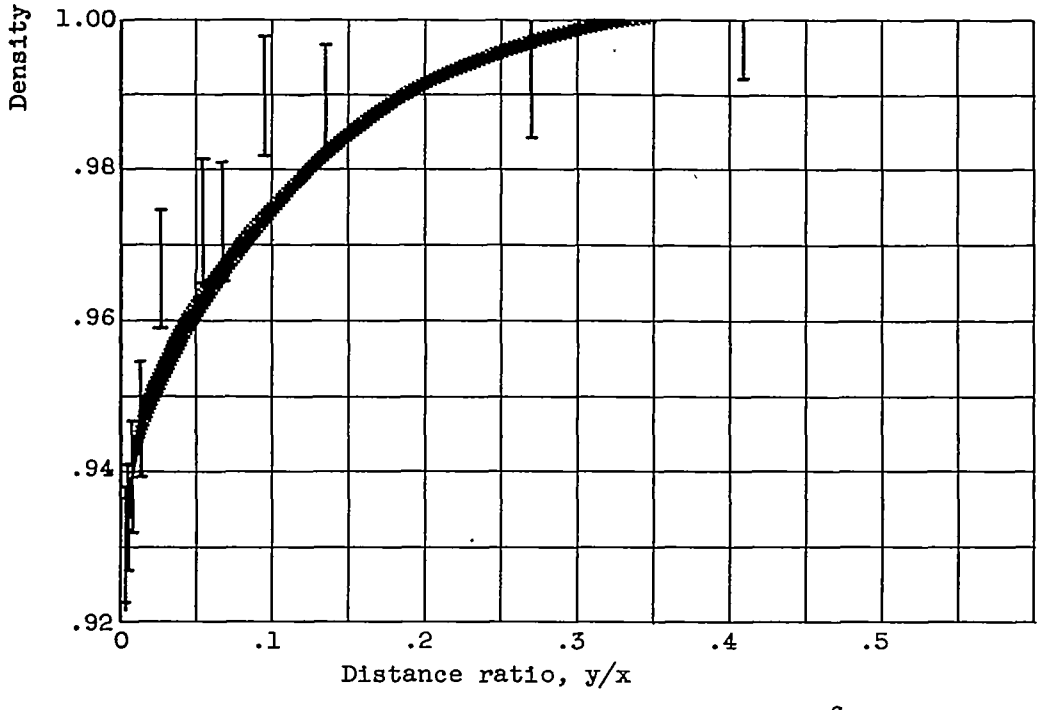

(b) Mach number, 0.78; Reynolds number, 2.3×10^6; static pressure, 20.0 inches of mercury; distance from leading edge of plate, 7.375 inches.

Figure 5. - Density distribution of turbulent boundary layer.

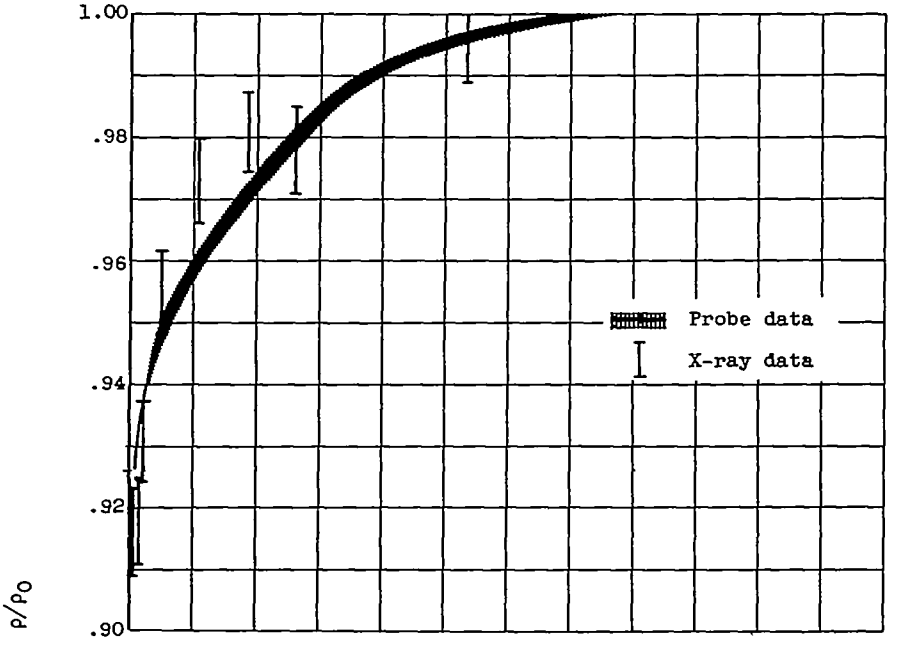

(c) Mach number, 0.78; Reynolds number, 1.7×10^6; static pressure, 15.0 inches of mercury; distance from leading edge of plate, 7.375 inches.

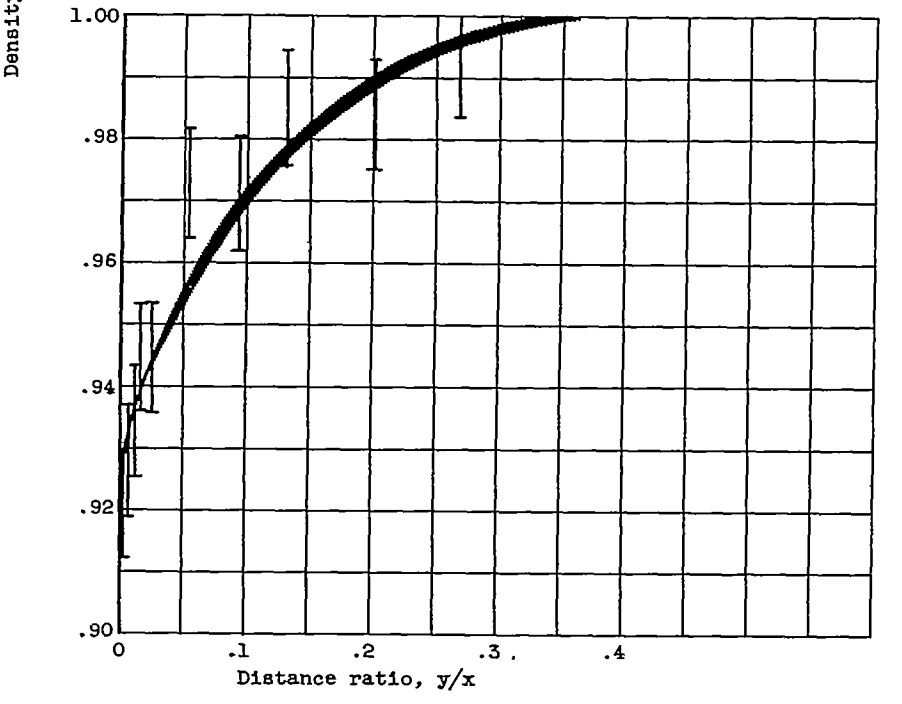

(d) Mach number, 0.78; Reynolds number, 1.1×10^6; static pressure, 9.9 inches of mercury; distance from leading edge of plate, 7.375 inches.

Figure 5. - Continued. Density distribution of turbulent boundary layer.

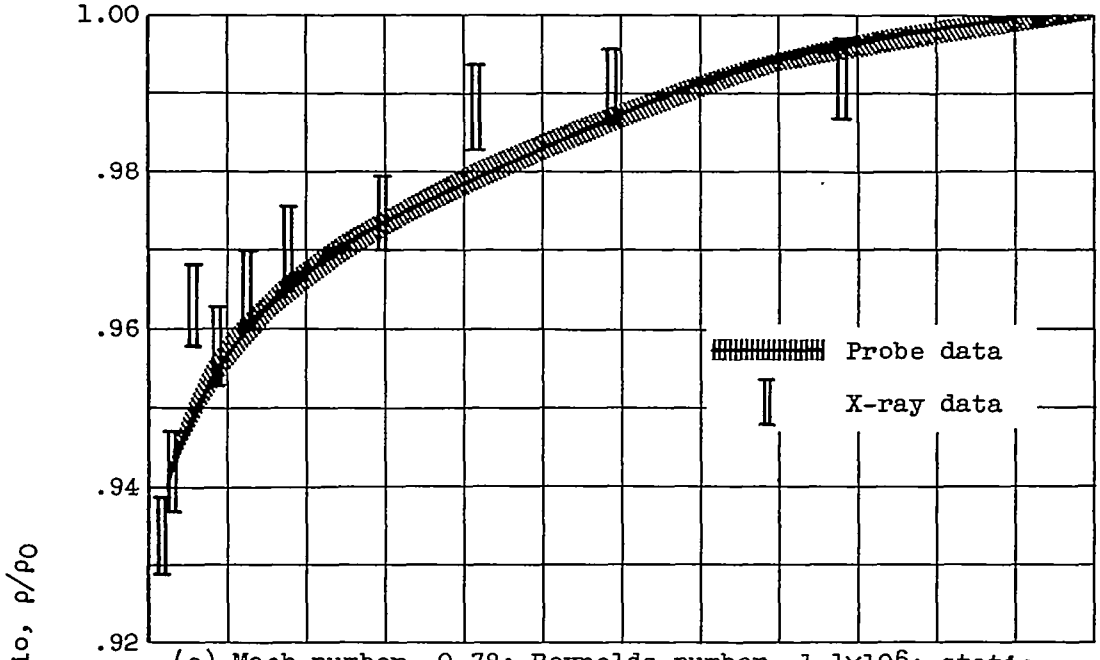

(e) Mach number, 0.78; Reynolds number, 1.1×10^6; static pressure, 20.0 inches of mercury; distance from leading edge of plate, 3.375 inches.

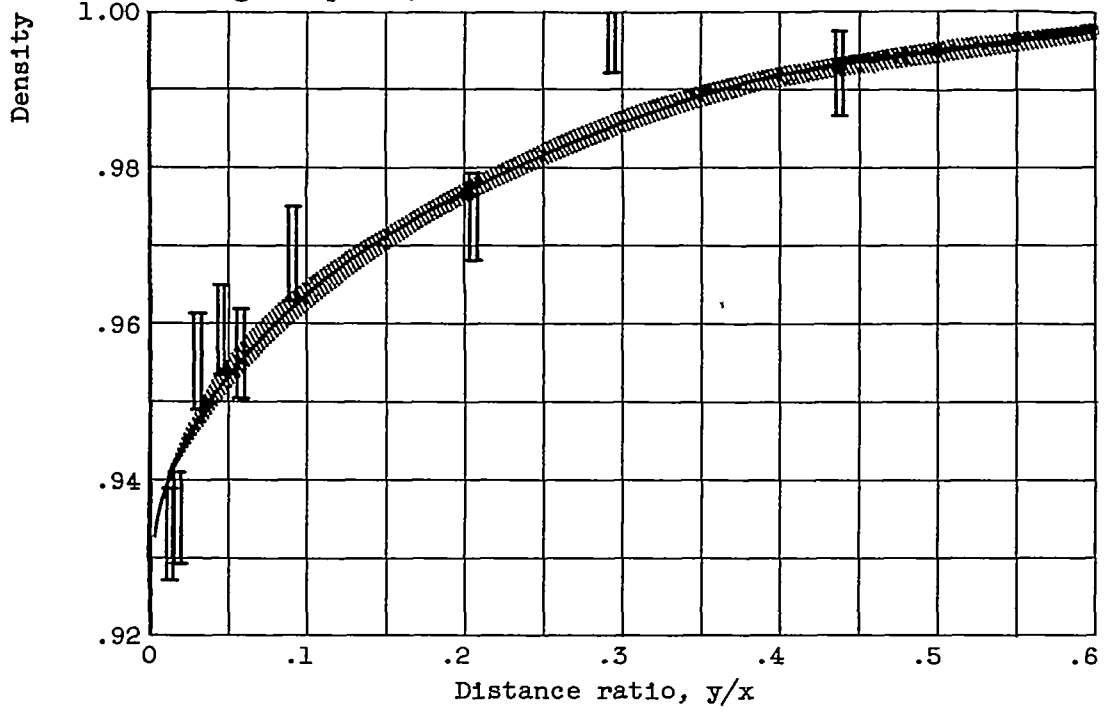

(f) Mach number, 0.78; Reynolds number, 0.5×10^6; static pressure, 10.3 inches of mercury; distance from leading edge of plate, 3.375 inches.

Figure 5. - Continued. Density distribution of turbulent boundary layer.

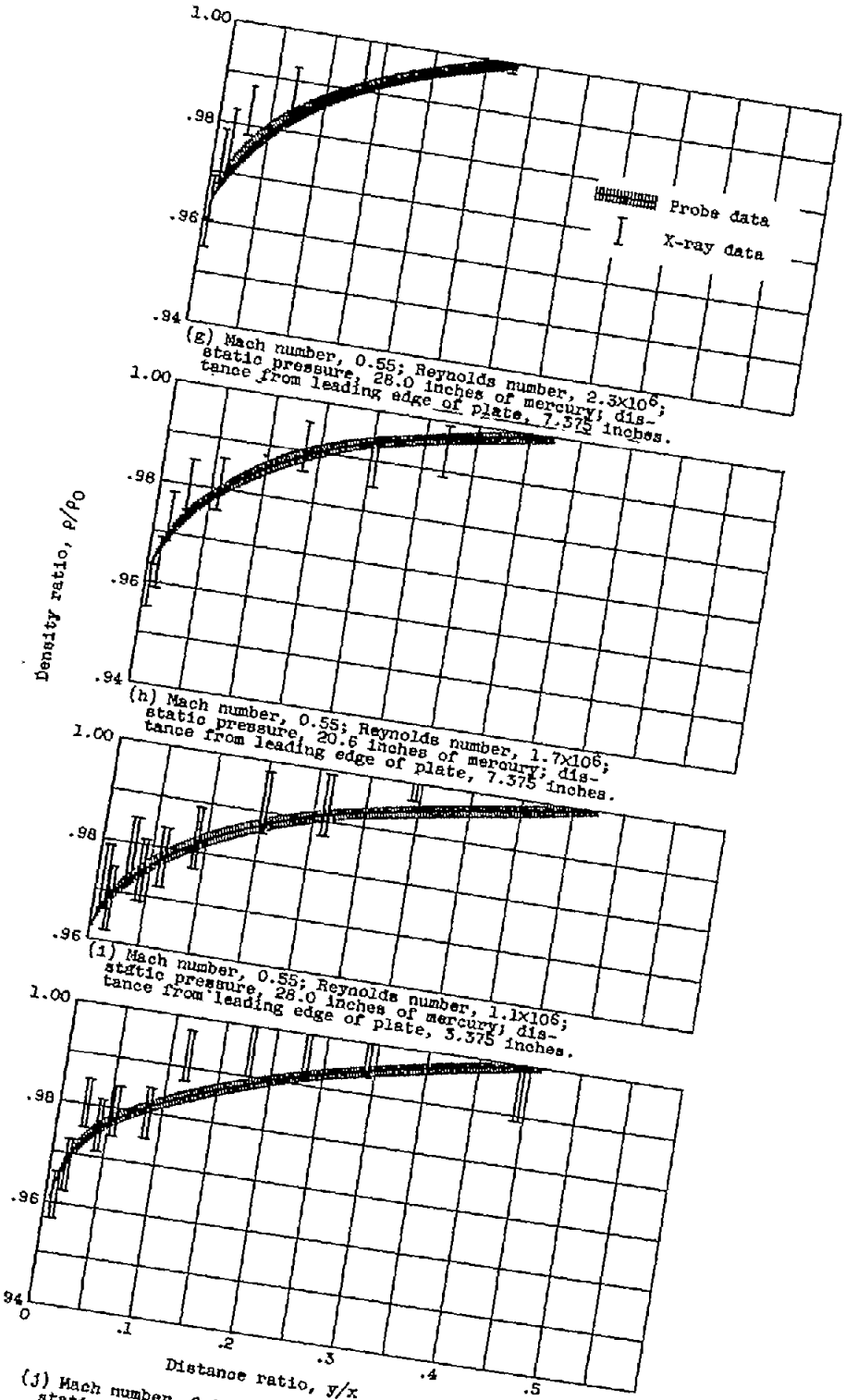

(g) Mach number, 0.55; Reynolds number, 2.3×10^6; static pressure, 28.0 inches of mercury; distance from leading edge of plate, 1.375 inches.

(h) Mach number, 0.55; Reynolds number, 1.7×10^6; static pressure, 20.6 inches of mercury; distance from leading edge of plate, 7.375 inches.

(i) Mach number, 0.55; Reynolds number, 1.1×10^6; static pressure, 28.0 inches of mercury; distance from leading edge of plate, 3.375 inches.

(j) Mach number, 0.55; Reynolds number, 0.5×10^6; static pressure, 13.8 inches of mercury; distance from leading edge of plate, 3.375 inches.

Figure 5. - Concluded. Density distribution of turbulent boundary layer.

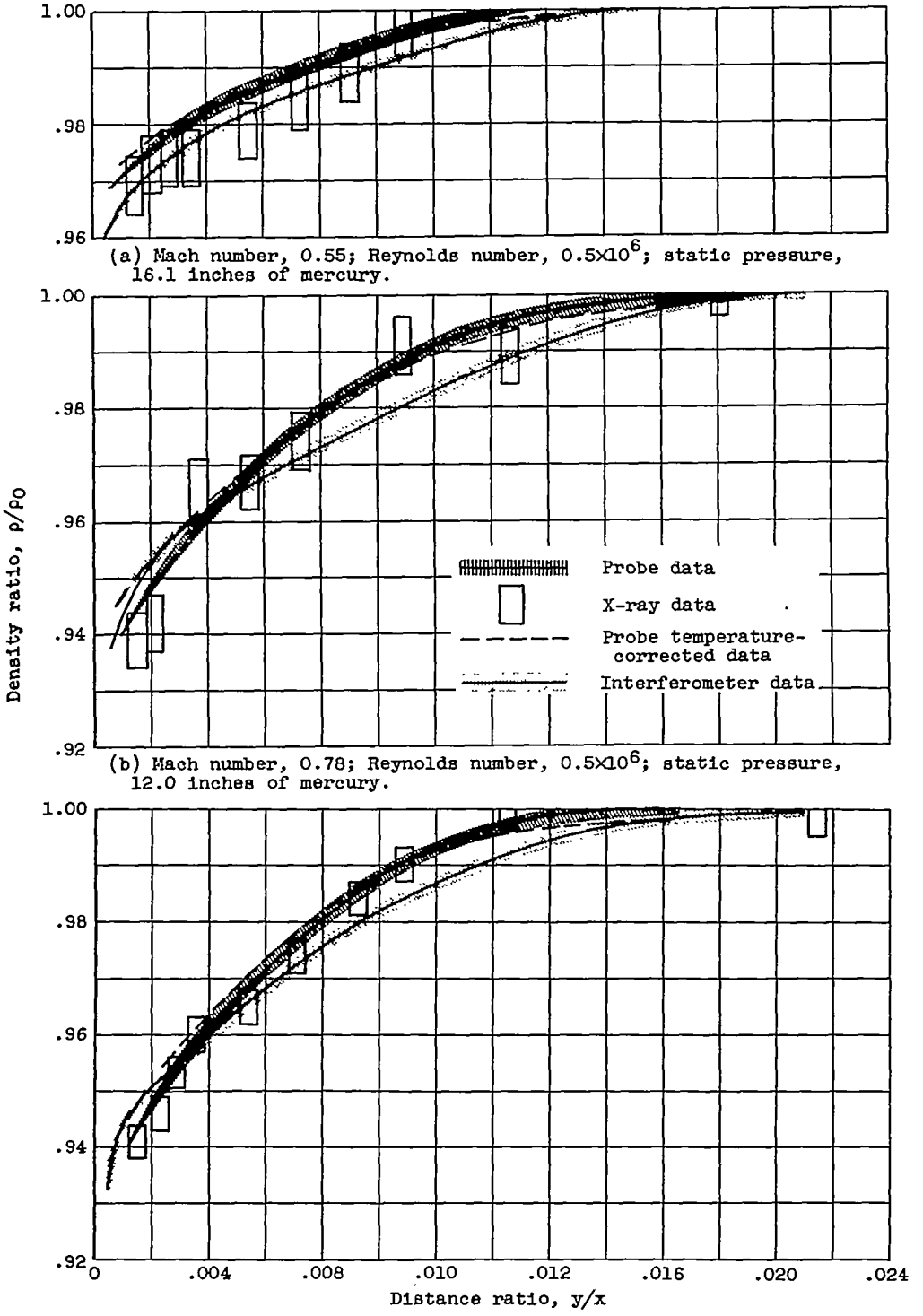

(a) Mach number, 0.55; Reynolds number, 0.5×10^6; static pressure, 16.1 inches of mercury.

(b) Mach number, 0.78; Reynolds number, 0.5×10^6; static pressure, 12.0 inches of mercury.

(c) Mach number, 0.78; Reynolds number, 1.1×10^6; static pressure, 25.3 inches of mercury.

Figure 6. - Density distribution of transitional boundary layer. Distance from leading edge of plate, 2.74 inches.

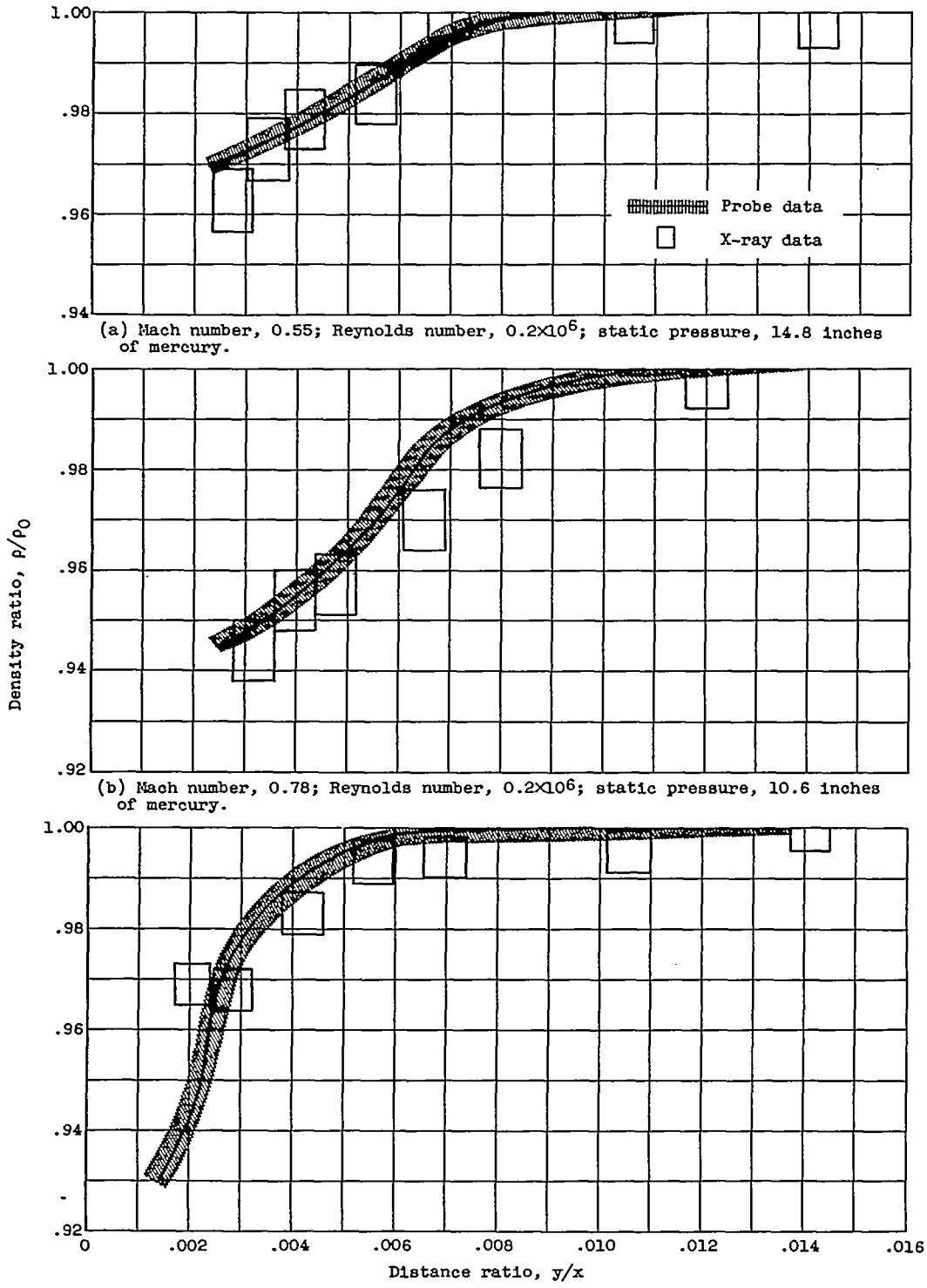

Figure 7. - Density distribution of laminar boundary layer. Distance from leading edge of plate, 1.24 inches.

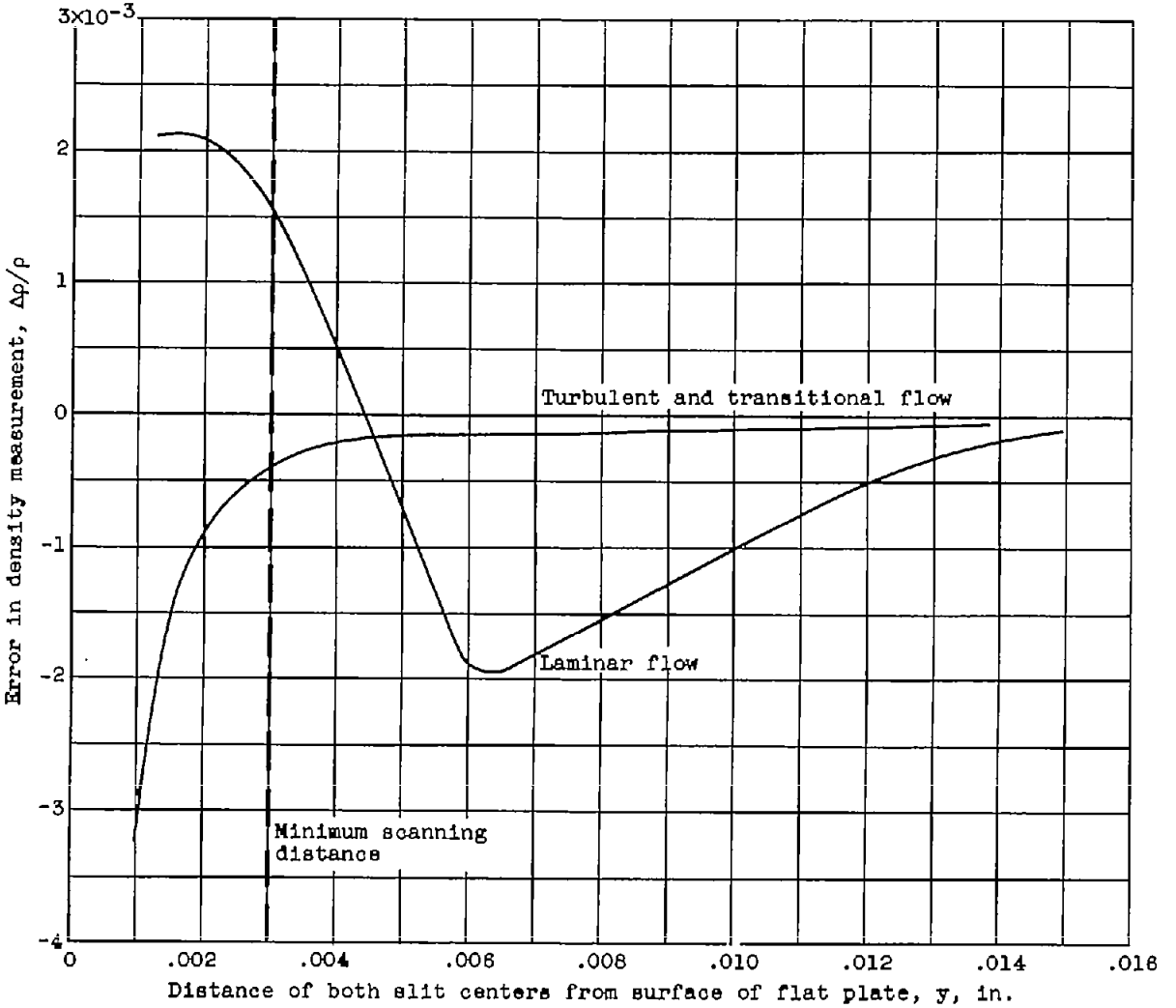

Figure 8. - Errors due to slit width. Exit slit, 0.005 inch; entrance slit, 0.010 inch; evacuated path, 3.8 inches; tunnel span, 3.8 inches.

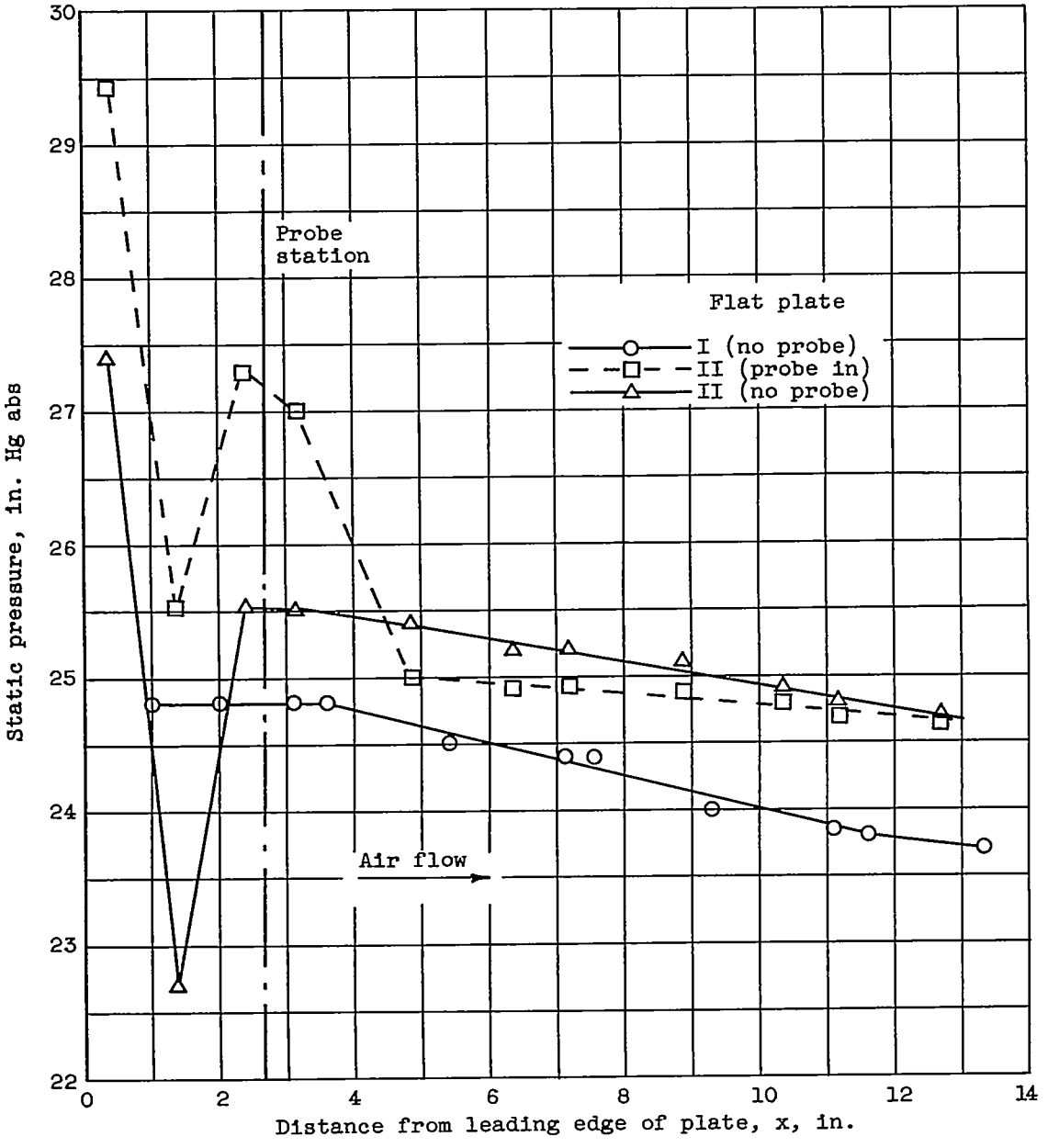

Figure 9. - Static-pressure distribution on flat plates I and II. Mach number with probe retracted, 0.78.

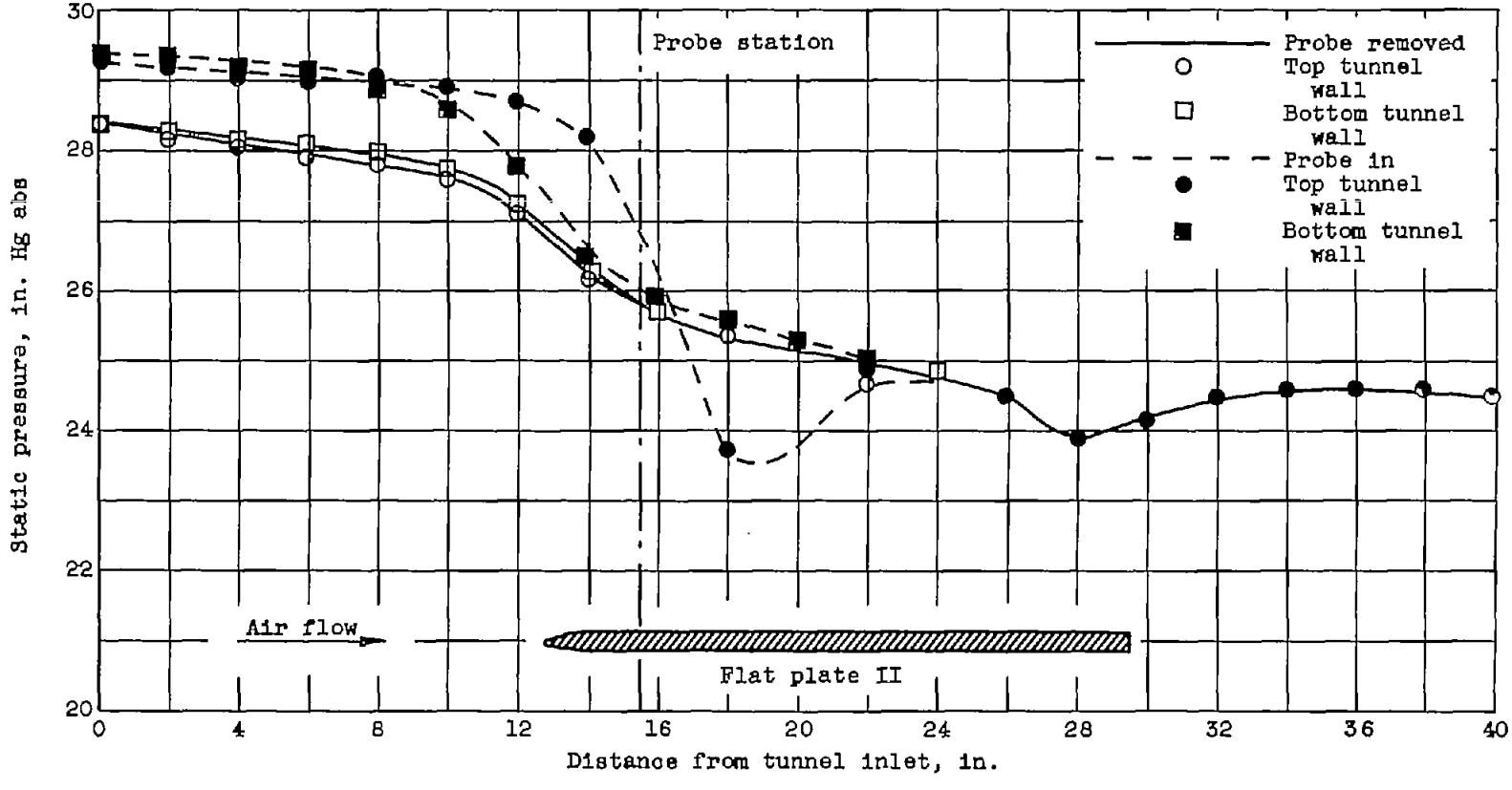

Figure 10. - Static-pressure distribution on tunnel walls with and without probe. Mach number with probe removed, 0.78; Mach number with probe in, 0.71.

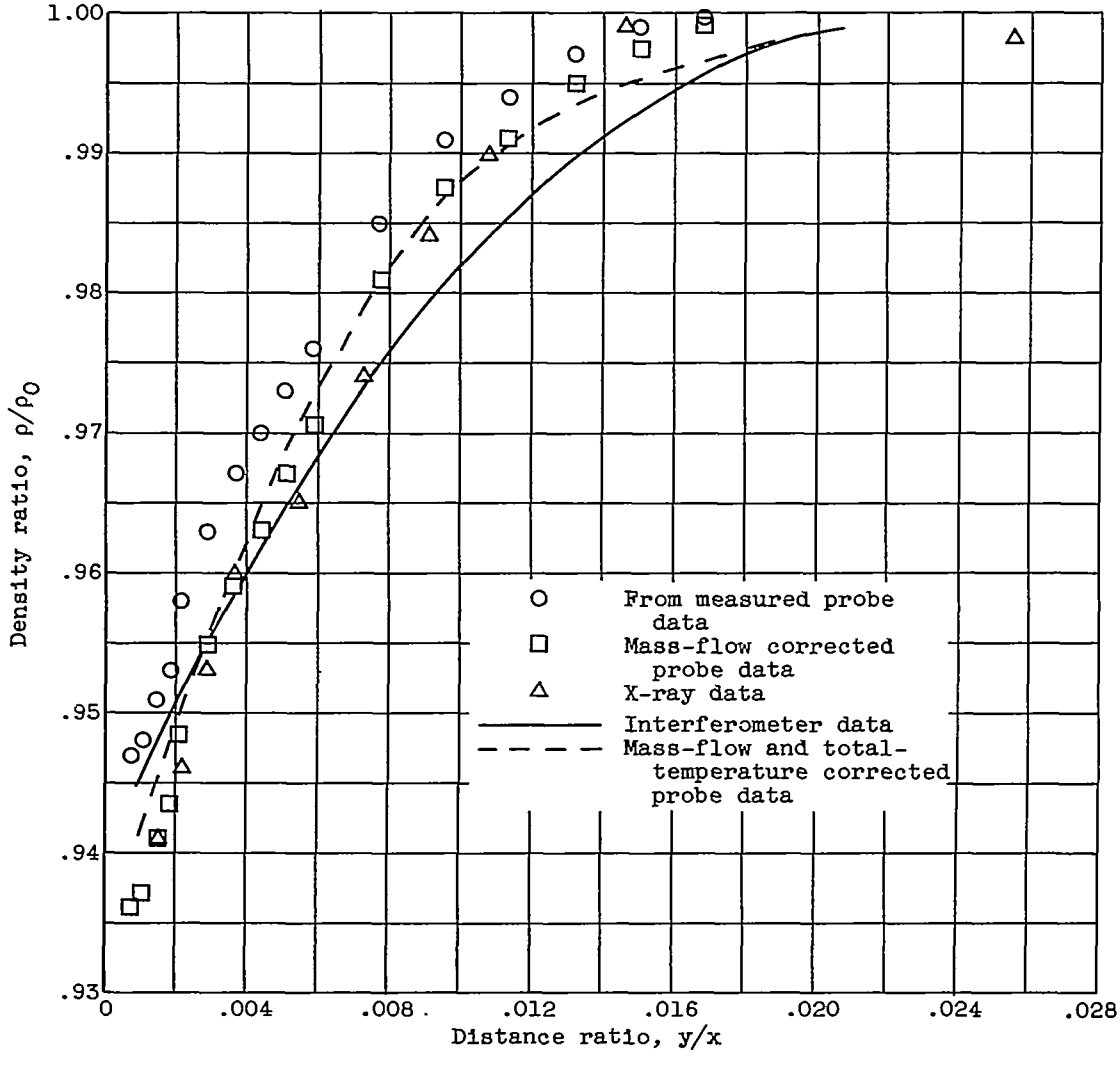

Figure 11. - Density distribution of transitional boundary layer. Flat plate II; distance from leading edge, 2.74 inches; Reynolds number, 1.1×10^6; Mach number without probe, 0.78; Mach number with probe, 0.71.

NACA-Langley - 2-4-54 - 1000